JOURNAL OF GEOPHYSICAL RESEARCH, VOL. , NO. , PAGES 1–27,

CTM Ozone Simulations for Spring 2001 over the Western Pacific: Comparisons with TRACE-P lidar, ozonesondes and TOMS columns

Oliver Wild,[1] Jostein K. Sundet,[2] Michael J. Prather,[3] Ivar S. A. Isaksen,[2] Hajime Akimoto,[1] Edward V. Browell,[4] and Samuel J. Oltmans[5]

O. Wild, Frontier Research System for Global Change, 3172-25 Showa-machi, Kanazawa-ku, Yokohama, Kanagawa 236-0001, Japan. (oliver@jamstec.go.jp)

[1]Frontier Research System for Global Change, Yokohama, Japan.

[2]Department of Geophysics, University of Oslo, Oslo, Norway.

[3]Earth System Science, University of California, Irvine, California, USA.

[4]NASA Langley Research Center, Virginia, USA.

[5]NOAA/CMDL, Boulder, Colorado, USA.

Abstract. Two closely related chemical transport models (CTMs) employing the same high-resolution meteorological data (∼180 km x ∼180 km x ∼600 m) from the European Centre for Medium-Range Weather Forecasts are used to simulate the ozone total column and tropospheric distribution over the western Pacific region that was explored by the NASA Transport and Chemical Evolution over the Pacific (TRACE-P) measurement campaign in February-April 2001. We make extensive comparisons with ozone measurements from the lidar instrument on the NASA DC-8, with ozonesondes taken during the period around the Pacific Rim, and with TOMS total column ozone. These demonstrate that, within the uncertainties of the meteorological data and the constraints of model resolution, the two CTMs (FRSGC/UCI and Oslo CTM2) can simulate the observed tropospheric ozone and do particularly well when realistic stratospheric ozone photochemistry is included. The models have the greatest difficulty reproducing the observations in the polluted boundary layer, where problems related to the simplified chemical mechanism and inadequate horizontal resolution are likely to have caused the net overestimation of about 10 ppb mole fraction. In the upper troposphere, the large variability driven by stratospheric intrusions makes agreement very sensitive to the timing of meteorological features.

1. Introduction

The NASA Transport and Chemical Evolution over the Pacific (TRACE-P) measurement campaign over the western Pacific region in Spring 2001 provided a comprehensive data set of tropospheric trace gases and their chemistry from a combination of aircraft, ground-based, and satellite platforms [*Jacob et al.*, this issue]. The objectives of the mission were to determine the pathways for outflow of trace gases, aerosols and their precursors from eastern Asia, and to study the subsequent chemical evolution of this outflow over the western Pacific. A major focus was on the production and export of ozone from this industrial region. Recent increases in emissions over the heavily populated and rapidly developing parts of East Asia are known to be large [*van Aardenne et al.*, 1999] and may have a significant global influence on air quality [*Jacob et al.*, 1999] and climate [*Berntsen et al.*, 1996]. The effects of East Asian sources on ozone over the U.S. and Europe are predicted to be greatest in early Spring [*Berntsen et al.*, 1996; *Wild and Akimoto*, 2001]. During TRACE-P, in-situ measurements of ozone from the NASA DC-8 and P-3B aircraft and tropospheric profiles from the DC-8 lidar [*Browell et al.*, this issue] were complemented by frequent ozonesondes from nine sites around the Pacific [*Oltmans et al.*, this issue], and by total ozone column data from the Earth Probe TOMS satellite instrument.

This rich dataset provides an exceptional opportunity to test current knowledge of ozone chemistry and transport within the framework of chemical transport models (CTMs) and specifically to assess the success of current models with appropriate meteorology in reproducing the observed ozone distribution. The region and period of the campaign provide particularly challenging conditions. The meteorological conditions in springtime over the western Pacific are characterized by the frequent passage of low pressure systems [*Fuelberg et al.*, this issue], which interlace continental air masses with cleaner, marine air from the tropical western Pacific. The sharp

rise in temperature and increasing insolation during springtime over East Asia lead to rapidly increasing photochemical activity. This coincides with the annual peak in emissions of ozone precursors from biomass burning sources in southern Asia, contributing to the large variability in ozone abundances over the western Pacific. Furthermore, the flux of stratospheric air into the troposphere in the Northern Hemisphere is greatest in Spring, and much of this influx occurs in tropopause folds associated with deviations of the jet stream that are most common over northeast Asia in springtime [*Austin and Midgley*, 1994]. Successful simulation of the ozone distribution over the region and its variability therefore requires a good treatment of stratosphere-troposphere exchange as well as of tropospheric photochemistry and the fluctuations in transport driven by frontal systems.

In this paper, we describe the use of two closely related CTMs (FRSGC/UCI and Oslo CTM2) driven by the same off-line meteorological data to simulate the tropospheric ozone distribution over the western Pacific in Spring 2001. These two CTMs are based on the same dynamical framework and tracer transport algorithms [*Prather*, 1987; *Prather et al.*, 1987] but run different chemical schemes, and thus allow a clear evaluation of the uncertainties introduced by the chemical model formulation. The meteorological data is unique to these studies and has been generated to provide a more self-consistent, continuously integrated, and higher temporal resolution global set of meteorological fields as compared with others available for this period. In addition, both CTMs contain treatments of stratospheric ozone using the schemes of *McLinden et al.* [2000], so that the influx of stratospheric ozone is predicted from the meteorological fields. In addition, with the Linoz scheme used in the FRSGC/UCI CTM we simulate the full variation of the total ozone column, tropospheric photolysis rates, and the stratosphere-troposphere ozone

net flux without imposing fixed ozone distributions or other artificial boundary conditions, still commonly used in tropospheric CTMs.

The goals of the paper are: (i) to document the meteorological data; (ii) to demonstrate that current tropospheric CTMs can simulate tropospheric ozone distributions and total ozone columns very well, even in conditions of high temporal and spatial variability; and (iii) to examine the accuracies and biases of these simulations in light of the available measurements. In section 2 we provide an overview of the two CTMs used and the meteorological data generated to drive them. In section 3 we evaluate the calculated ozone distributions and columns against those observed from the various measurement platforms available during TRACE-P and compare the performance of the two models. In section 4 we review the accuracy and biases of the modelled ozone with an in-depth look at the effect of spatial-temporal errors in the meteorological fields at scales comparable to the model resolution. In section 5 we conclude with a discussion of the directions needed to address the identified biases and to build confidence in our quantitative simulation of the sources and sinks that control tropospheric ozone.

2. Models and Meteorology

The global CTMs used here are the Frontier Research System for Global Change (FRSGC) version of the University of California, Irvine (UCI) CTM [*Wild and Prather*, 2000; *Wild and Akimoto*, 2001], and the University of Oslo CTM2 [*Sundet*, 1997; *Gauss et al.*, 2002]. These off-line CTMs maintain a common framework in terms of their use of meteorological data, tracer advection and convection [*Prather*, 1986; *Prather et al.*, 1987], and in their choice of boundary-layer treatments [*Hannegan*, 2000]. The horizontal and vertical resolution of the CTM is taken directly from (or is a subset of) the meteorological datasets, which supply advective and convective mass fluxes, temperature, pressure, humidity, precipitation, cloud water and a variety

of surface parameters for controlling treatment of deposition and boundary-layer turbulence. In the present study the Oslo CTM2 uses the option of the K-profile scheme of *Holtslag et al,* [1990], while the FRSGC/UCI CTM adopts the option of bulk mixing throughout the depth of the boundary layer every hour.

The principal difference between the models is in their treatment of tropospheric chemistry. The FRSGC/UCI CTM uses the ASAD package [*Carver et al.*, 1997] with a simplified hydrocarbon oxidation scheme and an implicit integrator; the Oslo CTM2 adopts the scheme of *Berntsen and Isaksen* [1997] with chemical integration using the QSSA approach [*Hesstvedt et al.*, 1978]. Both models calculate photolysis rates on-line with the Fast-J scheme [*Wild et al.*, 2000], with a full treatment of scattering by cloud droplets based on supplied cloud water and ice contents. Neither model contains a treatment of heterogeneous chemistry. While both models reproduce the mean distributions of tropospheric ozone and its precursors in the current atmosphere reasonably well [*Prather and Ehhalt*, 2001], the responses of the chemical systems are expected to differ at the smaller temporal and spatial scales examined here.

Global anthropogenic emissions of NOx, CO and hydrocarbons are taken from the EDGAR database for 1990 [*Olivier et al.*, 1996] for the FRSGC/UCI CTM and from the 1995 database [*Olivier and Berdowski*, 2001] for the Oslo CTM2. In both models, emissions over southern and eastern Asia are replaced with those for 2000 developed specifically for the TRACE-P campaign [*Streets et al.*, this issue]. Natural emissions are taken from the GEIA database. For biomass burning sources, both models use annual emissions from the EDGAR datasets; the FRSGC/UCI CTM applies climatological monthly variations according to *Wang et al.* [1998], while the Oslo CTM2 uses variations from *Andreae and Merlet* [2001].

In the stratosphere, the FRSGC/UCI CTM includes a simple treatment of chemistry using the Linoz scheme [*McLinden et al.*, 2000], a linearization of ozone production and loss in the present-day stratosphere (specified as a function of latitude, altitude and season) that accounts for varying temperature, local ozone abundance, and overhead ozone column. The 120 ppb mole fraction isopleth of the Linoz tracer is used to diagnose the dynamical tropopause and provides a self-consistent, four-dimensional tracer tropopause. In addition, the Linoz tracer provides a demarcation of stratospheric air, a more valuable quantity than tropopause height because the tropopause folds encountered during TRACE-P make the definition of a tropopause height ambiguous. The selection between tropospheric and stratospheric chemistry is make in real time for each grid box; when the ozone abundance above 10 km exceeds 120 ppb, Linoz chemistry is used. The net annual flux of stratospheric ozone into the troposphere based on a year of T42 meteorology for 1997 run to steady state is 557 Tg/yr, within the range derived from observations of 550 $\pm$140 Tg/yr [*Olsen et al.*, 2001].

The Oslo CTM2 uses the synthetic ozone tracer Synoz [*McLinden et al.*, 2000], in place of a stratospheric chemistry, setting the annual mean net flux of ozone from the stratosphere into the troposphere at 545 Tg/yr. Synoz is implemented by having a uniform source of this tracer in the tropical middle stratosphere and having it conserved except for near-surface loss. This chemistry precludes comparison with observed column ozone and thus cannot be used to calculate photolysis rates. In addition to these tracers, both CTMs carry a tracer of pseudo-stratospheric ozone that predicts the abundance of tropospheric ozone with a stratospheric source. This pseudo-stratospheric ozone has the stratospheric chemistry of Linoz/Synoz and in the troposphere is removed by chemical loss derived from the local chemical rates. While this is not a correct linearization of the impact of an added flux of stratospheric ozone, it provides a better indication

of stratospheric influence than that available using potential vorticity, which is destroyed in the troposphere by quite different mechanisms from that of ozone.

The meteorological fields for November 2000 to April 2001 are generated at the European Centre for Medium-Range Weather Forecasts (ECMWF) using the Integrated Forecast System (IFS) model version 23r4. The horizontal resolution chosen is the same as that for the ERA-40 data set, TL159 (i.e., N80), but uses 40 levels in the vertical, from the surface to 10 hPa, the standard vertical resolution of earlier IFS models. An optimal set of data for driving CTMs has been selected, and involves extraction of integrated convective fluxes and three-dimensional rainfall information from the IFS model in addition to the standard diagnostics. The use of forecast fields allows the treatment of convection to be fully consistent with the large-scale transport fields, precluding the need to derive convective processes off-line. The meteorological fields used here are a sequence of pieced forecasts; for each day, the IFS is initialized from analyses, a 36-hour forecast is run, and the final 24 hours are integrated and stored at 3-hour resolution. The initial 12-hour spin-up period is required to allow the model fields to adjust and is found to be particularly important for convective rainfall and for boundary-layer structure; however, such a spin-up period is far too short for the stratosphere and may lead to spurious vertical transport across the tropopause [*Douglass et al.*, 1996]. While it would be possible to piece together shorter forecasts to get the meteorology for each day (e.g., four 6-hour forecasts), ECMWF statistics suggest that objective forecast skills are as good after 36 hours as after 24 hours, and we assume that this also holds for the tracer transport fields. The large-scale winds, temperature and pressure are diagnosed as spectral coefficients; other parameters are collected as grid-point data. The notable strengths of these fields over other analysis products available

are their dynamical self-consistency, the use of integrated or averaged quantities, the range of diagnostics selected, and the higher temporal resolution.

For the present chemical studies over the TRACE-P period, the horizontal resolution is degraded to T63 (1.875° x 1.875°). The Oslo CTM2 uses the full 40 levels with a surface level thickness of about 16 m, but the FRSGC/UCI CTM adapts these to 37 levels, amalgamating the lowest 5 levels into 2 levels of thickness about 80 m and 120 m. Both CTMs have a mean vertical spacing of about 500 m at 500 hPa, increasing slowly to about 1200 m at 100 hPa.

3. Comparison with Observations

A major goal of TRACE-P is to understand the export of ozone and its precursors from industrial regions in eastern Asia. As part of that evaluation, this paper focuses simply on our overall simulation of tropospheric ozone abundance for the mission. Other analyses are necessary to assess the budget of tropospheric ozone. For example, carbon monoxide (CO) provides critical clues on the emissions and model meteorology [*Kiley et al.*, this issue]. Analysis of our model simulations of ozone precursors and other tracer species measured from the two aircraft will likely give us more confidence that we have correctly identified the regions of ozone production. Indeed, the biases identified in this first analysis point to regions where more extensive analysis is needed.

3.1. TOMS Columns

The total ozone column is available on a daily basis from the Earth Probe Total Ozone Mapping Spectrometer (TOMS) instrument. Inclusion of the Linoz stratospheric chemistry for ozone in the FRSGC/UCI CTM allows us to simulate the total column and its full variability. The Oslo

CT**M**2 applies the Synoz formulation which does not aim to reproduce the total column and cannot be used here.

Figure 1

Figure 1 shows the latitudinal gradient in ozone column over the western Pacific region in March 2001 from TOMS and the FRSGC/UCI CTM. The vertical bars show the rms variance over the range of longitudes and time. As good coverage from TOMS is only available on a daily basis, the means and variability are derived from the daily columns. The latitudinal gradient over the western Pacific region is reasonably well reproduced, with columns below 250 Dobson Units (DU) in sub-tropical regions rising to more than 450 DU at 45°N. While the mean columns are overestimated at high latitudes by up to 12%, and underestimated at low latitudes by up to 8%, the gradient at mid-latitudes is well reproduced, and the variability, rising from 4% to about 15% with increasing latitude, is very well matched.

Figure 1 also shows the ozone column as a function of latitude for all longitudes (dashed lines), and demonstrates the significant longitudinal structure in column ozone with much higher values over the western Pacific at mid-latitudes. A steeper latitudinal gradient is found over the western Pacific, with larger columns north of 30N. This high latitude enhancement and low latitude reduction in regional ozone column compared with the global zonal mean is captured very well in the model. The difference between the regional and global latitudinal gradients also suggests that use of a zonal mean column climatology would produce a systematic bias in this region. The bias in the simulated ozone columns, however, highlights a problem with the chemistry at the 10% level, or, more likely, in the stratospheric residual circulation of the pieced IFS meteorological fields. A similar tendency to overestimate mid-latitude ozone columns is found for a number of models using assimilated wind fields [*Douglass et al.*, 1996; *Bregman et al.*, 2001].

To examine the spatial variability and the timing of the passage of major features, we present a sequence of ozone columns over the western Pacific region during Spring 2001 from the FRSGC/UCI model synchronized with TOMS columns from successive orbits of the Earth Probe satellite. The movie[1] shows the evolution of the total column, and demonstrates that the largest variations, driven by the passage of low pressure systems and the movements of the jet stream, are captured well by the model, both spatially and temporally. Some examples are shown in Figure 2, highlighting the large columns north of Japan and the cut-off vortices which sometimes occur over the eastern Pacific, and which often re-attach to the main stream further downwind. Many of these features are reproduced well by the model, and their evolution provides additional information to interpret the daily snapshots provided by TOMS. Overestimation of the columns at higher latitudes typically occurs in the fold regions behind low pressure systems, and causes the diagnosed tropopause height in these regions to be too low. Despite this discrepancy, the short-term and small-scale variations in the total column are well reproduced, and hence it appears that dynamical impacts on the lower stratospheric ozone distribution are well represented in the FRSGC/UCI CTM using Linoz and the EC IFS 40-level pieced-forecast meteorological fields. In this comparison, it is important to look at the hourly simulations against the satellite over-passes as shown in the movie, not just at the daily TOMS maps.

movie

Figure 2

As the annual net flux of ozone from the stratosphere to the troposphere is reproduced very well, the success in capturing total column variations suggests that the model is in a good position to correctly simulate the mechanisms for exchange of air across the tropopause, and hence to capture the influx of stratospheric ozone during the TRACE-P campaign.

3.2. Ozonesondes

Profiles of ozone over the western Pacific in Spring 2001 are available from frequent ozonesonde launches over Japan, Korea, Taiwan and Hong Kong, with additional sondes over the eastern Pacific from Hawaii and California [*Oltmans et al.*, this issue], see Table 1. In terms of ozone peaks throughout the troposphere, many of the soundings captured intrusions of stratospheric air in the upper or mid-troposphere, apparent evidence of stratospheric influence at lower altitudes, and highly polluted continental air in the boundary layer. We first use the data to examine the model simulations of the vertical profile, and then focus on tropopause heights and boundary layer ozone.

Table 1

The tropospheric structure on selected profiles during the campaign period is shown in Figure 3. Both ozonesonde and model profiles show a high degree of variability in space and time, with significant layering near the surface and in the upper troposphere. Agreement between the modelled and measured profiles is quite good; key features are generally correctly located, and magnitudes are reproduced reasonably well. In a few cases features are missed, such as the upper tropospheric layer over Hong Kong on March 29, or are greatly underestimated, as for the layer over Taiwan and Hong Kong on March 16; these may reflect errors in the timing of meteorological features or variability in chemical production from episodic sources such as biomass burning. In some cases complex profiles are reproduced, but with small shifts in location and magnitude. The profile at Naha on March 6 shows three distinct layers, and the models indicate that the upper and lower layers are heavily influenced by stratospheric air while the middle layer has a more recent chemical origin.

Figure 3

Agreement between the models is usually good at low latitudes, but rather poorer over northeast Asia, principally due to the importance of stratospheric influence over this region. While the

tracer tropopause is often similar, the magnitude of intrusions is rather different. This is clearest during large intrusions such as that at Cheju on March 1, or at Kagoshima on March 13 and 22; the FRSGC/UCI CTM slightly overestimates stratospheric influence, while the Oslo CTM2 significantly underestimates it. At Sapporo on April 4, where a layer with strong stratospheric influence in the lower troposphere produced ozone enhancements of more than 40 ppb, the FRSGC/UCI CTM suggests an enhancement of about 30 ppb, while the Oslo CTM2 gives an enhancement of only 10 ppb. The stratospheric influence extends beyond situations with intrusions; the 10 ppb difference between the models in the lower troposphere over Taiwan on March 13 reflects differing stratospheric influence in dry descending air, and is not present on March 16 or 20 when the models agree much better. This suggests that a good treatment of stratospheric ozone distributions is required to successfully model ozone in the troposphere throughout the region. Specifically, the Synoz formulation, based on an annual mean flux from the stratosphere, may not be adequate for such detailed seasonal simulations.

Figure 4

Figure 4 shows the altitude distribution of the 150 ppb ozone isopleth from all sondes between February and April that reached the tropopause. This diagnostic reflects the height of the tropopause or of any large stratospheric intrusion present below this. For the FRSGC/UCI CTM, the variation in altitude is captured well, with just five or six cases where stratospheric intrusions were intercepted but are not found in the model, and a similar number found in the model but not in the observations. Most of these cases occur for Cheju and Tateno, close to the tropopause break around 35°N, and are principally due to spatial and temporal offsets in the meteorological fields; the impacts of this variation are examined in the following section. While the figure reflects the latitudinal gradient in mean tropopause heights, large stratospheric intrusions with ozone greater than 150 ppb found 5–6 km below the mean tropopause height are

successfully captured at Kagoshima, Naha and Hilo on many occasions. While the variation in height is captured very well, there is a net tendency to underestimate it by about 500 m (about half the thickness of a model level at 12 km). This is driven principally by the northeast Asian sites, and is consistent with the higher total columns found over the region, noted earlier.

The Oslo CTM2, using the Synoz formulation, captures the tracer tropopause well at the higher and lower-latitude sites, but underestimates the magnitude of the large intrusions that affect Tateno, Cheju and Kagoshima. In 10–15 cases, these intrusions do not reach 150 ppb of ozone, and the 150 ppb isopleth therefore reflects the height of the tropopause rather than that of the intrusion. Consequently, the 150 ppb diagnostic shown in Figure 4 is overestimated on these occasions. Examples of this can be seen in Figure 3 for Cheju on March 2 and for Kagoshima on March 13. In the absence of these sites, agreement is rather better, with a slope of 0.91 and r^2 of 0.88, but a net tendency to overestimate the height by about 1 km remains, reflecting an underestimation of the stratospheric contribution to background ozone in the upper troposphere.

High levels of ozone are seen in the boundary layer on a number of occasions, and while more extreme events, such as over Taiwan on March 16, are underestimated, there is a general tendency towards overestimation. In Figure 5, we show the mean ozone level in the boundary layer below 800 hPa from the ozonesondes and the models. In the FRSGC/UCI CTM, ozone levels are well matched in cleaner regions such as at Hilo, but are consistently overestimated at the Japanese sites by an average of 18 ppb. The most polluted cases with ozone up to 90 ppb occur for sites close to large urban sources, and may reflect local pollution episodes which are not captured by the model. Over all sondes, mean ozone in this layer is 45.0$\pm$12.2 ppb, while the model suggests 56.5$\pm$13.3 ppb, a net overestimation of almost 12 ppb. For the Oslo CTM2, diagnostics for Hilo are unavailable, and the correlation is consequently poorer. A similar overestimation of ozone

Figure 5

over the Japanese sites is seen, but is rather smaller than for the FRSGC/UCI CTM, typically less than 10 ppb. The mean sonde ozone is 48.3±12.9 ppb, compared with 52.7±5.6 from the model, a net overestimate of less than 5 ppb. The smaller tendency to overestimate boundary layer ozone in the Oslo CTM2 compared with the FRSGC/UCI CTM is seen in the second panel in Figure 5. However, the variability in ozone is not captured as well with the Oslo CTM2, and in the more polluted cases ozone is underestimated.

The tendency to overestimate ozone over the northeast Asian sites stems partly from the inherent inability of coarse-resolution models to capture the non-linearities in smog production of ozone, including NO_x loss, very close to source regions. It may also be due to errors in precursor emissions. The effect is larger for the FRSGC/UCI CTM, where the boundary layer mixing scheme further dilutes emissions. The Holtslag scheme in the Oslo CTM2 reduces this mixing, typically leading to less chemical production and a better vertical gradient. Overestimation is particularly bad over Japanese sites, as air arriving here has typically crossed major source regions over China and Korea, often in the strongly capped boundary layer behind a cold front, and hence these non-linearities are exaggerated. Agreement is somewhat better in both models over the southern sites such as Hong Kong, but modelled variability here is large, perhaps reflecting episodic influence from large local sources. Note also that the majority of sondes are launched in the afternoon, when photochemically produced ozone in the boundary layer may be at a maximum.

The stratospheric contributions to near-surface ozone are greater than those over much of the rest of the profile on a number of occasions, particularly over Taiwan and Hong Kong. Two examples from the FRSGC/UCI CTM are shown in Figure 6. This typically occurs on the southern side of high pressure systems, where stratospheric air brought down behind the cold

Figure 6

front of a preceding cyclone continues to subside to the lower troposphere over the ocean, and is brought to the coastal ozonesonde sites by low-level on-shore flow. Over Taiwan on March 13, there is a distinct layer of stratospheric influence below 800 hPa at the base of a dry, subsiding air mass capping the boundary layer; the sonde profile shows the same features. Similar conditions are seen over Hong Kong on March 16, although in this case the mid-troposphere is dominated by more humid westerly flow from continental regions which shows very little stratospheric influence; only in a dry layer at 400 hPa are stratospheric impacts again visible. Note that ozone from non-stratospheric sources is also elevated in the boundary layer, as local chemical production is supplemented by recirculation of polluted continental air transported over the ocean behind the previous cold front. While the simple boundary layer treatment used in the model may overestimate the mixing of stratospheric air to the surface, it is clear that stratospheric intrusions may strongly influence tropospheric ozone below 800 hPa in springtime even at these low latitudes.

The peak in ozone at 320 hPa over Hong Kong on March 16 is not captured well by either model (see also Figure 5). Although this layer is relatively dry, the models indicate that the stratospheric influence here is small. The location of the peak is captured better by the Oslo CTM2 than the FRSGC/UCI CTM, and the difference between the models here and similarity over the rest of the profile suggest a tropospheric origin due to different treatments of chemistry or emissions, rather than to miss-timing of an intrusion in the meteorological fields. Underestimation of ozone formation following precursor emissions from episodic sources such as biomass burning over southeast Asia, treated in a climatological sense in the present modelling studies, is the most likely reason for this discrepancy.

3.3. Lidar Profiles

The lidar instrument on the DC-8 aircraft provided high-resolution profiles of ozone through the depth of the troposphere for each flight during the campaign [*Browell et al.*, this issue]. We derive similar profiles from the models by following the flight tracks though model fields output at hourly resolution, and show examples of the comparison for the FRSGC/UCI CTM in Figure 7. We select two transit flights, one over the central Pacific and one over the North Pacific, and two flights over the western Pacific, one out of Hong Kong and one out of Yokota air-base, Japan. Cloud optical extinction derived from the meteorological data is also shown, as cloud droplets attenuate the beam of the lidar instrument, and hence account for many of the gaps seen in the data.

Figure 7

The ozone profiles on these flights differ greatly, dependent principally on the latitude and the meteorological features encountered. On flight 5, from Hawaii to Guam, the aircraft encountered a thick layer of polluted air of Asian origin covering a wide area of the central Pacific, overlying the clean marine boundary layer and capped by clean, subsiding air. This layer had become detached from the main westerly flow at higher latitudes due to the action of a strong frontal system bringing cleaner marine air from the southwest. The formation of this layer is reproduced successfully by the model, though peak ozone is underestimated by 5–8 ppb. Flight 7, out of Hong Kong, sampled air on both sides of a frontal system off the coast of China. Ahead of the front the air was relatively clean; while cloud cover in the vicinity of the front prevented clear profiles in the frontal region, the model shows high levels of ozone in the boundary layer outflow behind the front, and elevated levels of ozone at 8-10 km with both stratospheric and tropospheric components, suggesting filaments of dry stratospheric air interlaced with convective outflow. Ahead of the front again ozone levels are lower, though a persistent layer of tropospheric origin

is present at around 10 km in both model and measurement profiles. Flight 14, out of Yokota, sampled convective outflow over the western Pacific, interlaced with filaments of stratospheric air. Relatively high levels of ozone are found in the upper troposphere in the model, with a number of clear stratospheric intrusions encountered; however, there are also strong bands of continental outflow at 8–10 km, consistent with convective activity over Eastern China.

We consider in detail the features of the ozone distribution on flight 18, April 3–4, when the DC-8 flew from Japan to Hawaii. This flight involved two frontal crossings, and the lidar profiles show a high degree of structure, much of which is captured well by the model. The frontal crossings, at about 23:30 and 04:00 GMT, stand out clearly in the profiles shown in Figure 7 due to the sharp drop in ozone abundances on moving from regions behind the front, heavily influenced by subsidence of stratospheric air, to cleaner regions ahead. The large intrusion and heavy cloud cover associated with the younger frontal system to the west are captured well; a smaller intrusion at about 5 km is seen behind the mature system in the central Pacific. Stratospheric influence is also seen in two steeply-sloping filaments towards the end of the flight on the approach to Hawaii. To more clearly illustrate the main features of the ozone distribution, we show the stratospheric and tropospheric components of ozone from the modelled profiles in Figure 8. The location of the frontal systems, and their periodic nature, can seen in the 500 hPa surface of the stratospheric component, with large intrusions behind each front wrapping round the trailing anticyclone. The stratospheric ozone visible at 10°N 170°W is the remnant of an intrusion from a previous system trapped in the tropics; the tropopause fold leading to the creation of this intrusion is clearly visible at 170°W in the total ozone column on March 31, shown in Figure 2. The two filaments encountered towards the end of the flight are remnants of this intrusion. Continental outflow in the mid-troposphere is clearly visible between the frontal systems as high levels (>40 ppb) of the

Figure 8

tropospheric component of ozone, and results from both transport of polluted air previously lifted by convection, and from slower lifting associated with the fronts. Nearer the surface there is some recirculation of post-frontal outflow around the anticyclone, accompanied by a significant stratospheric component, although this is overestimated compared with the lidar profiles. Ahead of the eastern front, the lower troposphere is influenced by clean marine air masses, but higher ozone in the upper troposphere has a large component from East Asian sources that can be traced back to the continent 5–6 days earlier.

In summary, the model does very well simulating the highly variable distribution of ozone in the troposphere. The main discrepancies are in the boundary layer, where there is a tendency to overestimate abundances close to continental source regions as noted earlier, and in the upper troposphere south of 30°N, where episodic sources over southeast Asia such as biomass burning lead to occasional underestimation of ozone. The capping of the boundary layer behind cold fronts is rather strong, and contributes to the excess ozone build-up close to the surface in these simulations.

Note that the ECMWF IFS model captures the general features of the cloud fields quite well. While cloud cover is often very heterogeneous at small scales, and interception strongly dependent on the track of the aircraft, the model appears to capture the presence of larger-scale cloud decks well, particularly those associated with frontal systems. In many cases, such as on flights 7 and 14, these are corroborated by the flight log and clearly account for the lack of lidar data.

4. Evaluation of Biases and Accuracy

We have identified some clear systematic biases in the ozone simulations in terms of columns, boundary layer abundance, and tropopause heights. On the other hand, we have found a surprising

accuracy in simulating the fine structure of the ozone columns that are matched by the TOMS swaths. One aspect of the accuracy of these simulations that we have not examined is the spatial and temporal displacements of chemical or meteorological features that may be due to biases in emissions, chemical time scales, or phase errors in the driving meteorology. In this section we focus on the latter.

The timing and placement of major dynamical features in the IFS meteorological fields is generally good, as seen from the TOMS columns (Figure 2), ozonesonde profiles of humidity (Figure 6) and temperature (not shown), and the positioning of the major cloud decks encountered on the aircraft flights (Figure 8). Nevertheless, the calculated ozone distribution is sensitive to any deviations that may occur, particularly in the boundary layer close to continental source regions, where chemical ozone production and destruction may be fast, and in the upper troposphere, where variability is large due to the formation and passage of stratospheric intrusions.

To assess the sensitivity of ozone to this type of variability, we extend the ozonesonde comparisons with the FRSGC/UCI CTM by varying the sonde location by one or two grid boxes (2–4° in latitude or longitude), and by varying the sampling time by 6–12 hours. To investigate the impact of stratospheric intrusions, we focus on the region of greatest variability between 30 and 35°N, close to the jet stream and the tropopause break. Figure 9 shows the ozonesonde for Cheju (33.5°N) on March 1, 2001, together with the variability of the model profile in space and time. The simulated profile captures the ozonesonde profile well, with a thick stratospheric intrusion at 250 hPa reaching 120 ppb and a second stratospheric layer at 500 hPa which is broader in the model than in the observations. The shift in simulated profile with latitude demonstrates the presence of strong gradients. At the most northerly extent there is a single, broad intrusion peaking at 350 ppb at 200 hPa and filling the upper troposphere, while to the south the magnitude

Figure 9

rapidly drops off and two intrusions are seen, with peaks at 300 and 600 hPa. At the correct latitude, the model profile reproduces both the magnitudes of the ozone peaks and the altitudes of the layers. The longitudinal gradient is rather smaller, as expected; the upper branch of the intrusion weakens only slightly from west to east, but the lower branch, present at 600 hPa in the western profiles, vanishes on moving to the east. While boundary layer ozone is over-estimated in all these profiles, the more westerly ones, over the Yellow Sea and closer to source regions, show the greatest enhancements. The temporal variation over a 24-hour period is also large. The upper branch of the intrusion builds in magnitude and drops about 50 hPa; the lower branch is not visible in the first profile, and drops rapidly from 400 to 700 hPa, with an appropriate magnitude only at the correct sampling time. The baseline tropospheric ozone drops from 80 to 50 ppb at the end of this period, as the stratospheric influence is transported eastwards. Twenty-four hours later, on March 2, when a second ozonesonde was launched, these lower values are maintained, and the profile is essentially flat up to 250 hPa, where the upper branch of the intrusion is still visible. This shift in structure over 24 hours is simulated extremely well by the FRSGC/UCI CTM.

This case was selected for the observation of stratospheric intrusions and for the availability of distinct ozonesonde profiles on successive days. While it is broadly typical of our model simulations, intrusions are not reproduced as well in some other situations, as seen in Figure 4. Allowing a small degree of spatial and temporal shift in fitting the modelled profiles to the sondes to adjust for the phasing of the meteorology may therefore improve the agreement, as expected. This may provide the basis for a more quantitative measure of model performance in capturing profile structure, and is a goal of future research. Nevertheless, we demonstrate that in many

cases the structure is already reproduced well, with no systematic adjustment required to improve the fit, and conclude that there is no obvious spatial or temporal bias in the meteorological fields.

5. Conclusions

This paper has introduced and characterized two CTMs (FRSGC/UCI and Oslo CTM2) that are being used to examine the chemical environment over the western Pacific in Spring 2001, with the goal of quantifying the impacts of Asian outflow on regional and global scales. We have described the meteorological data used to drive these models, generated with the ECMWF IFS model specifically for the TRACE-P campaign, and have demonstrated that the general features of the tropospheric ozone distribution due to both tropospheric and stratospheric sources are captured very well.

Application of a linearized stratospheric photochemistry for ozone production and loss (Linoz) allows us to model successfully the total ozone column and its short-term variability and appears to be much better than simpler approaches. The consequent self-consistency of stratospheric ozone with the dynamical features of the tropopause region allows a more realistic simulation of stratospheric intrusions. From comparisons with both ozonesondes and lidar measurements, this stratosphere-troposphere interface is reproduced well over the western Pacific in the Spring 2001 period. Use of a simpler, synthetic ozone tracer (Synoz) leads to underestimation of the magnitude of intrusions in this region in springtime, even though the total annual cross-tropopause flux is appropriate. A detailed comparison with measurements suggests that the tropopause heights diagnosed using the Linoz chemistry are slightly too low, and that the total ozone column north of 35°N is too large. This is likely due to a more vigorous stratospheric overturning, and similar excess fluxes of stratospheric ozone with assimilated fields are noted by others [*Douglass et al.*, 1996].

Ozone in the boundary layer over northeast Asia is generally overestimated in both models. We believe that a large part of this bias is due to overestimated chemical formation associated with the dilution of precursor emissions within a model grid box inherent to coarse-resolution Eulerian models. The overestimation is worse in the FRSGC/UCI CTM, where complete mixing of the boundary layer occurs every hour; in the Oslo CTM2, which maintains vertical gradients within the boundary layer, there is less efficient ozone production. However, other factors, such as errors in precursor emissions, strong boundary layer capping in outflow behind fronts, and overestimation of stratospheric influences, may also contribute. In clean conditions, such as at Hilo, the models perform better. We will need to examine the ozone bias with respect to other tracers from ozone source regions to resolve this uncertainty.

The meteorological fields used in the models capture the general structure and timing of the cyclonic systems that affect the western Pacific region. We demonstrate the large variability in ozone that may occur on relatively small temporal and spatial scales. Allowing for small space-time errors in the phasing of the meteorology can in a few cases lead to better agreement with observations, although there is no obvious systematic bias. Further evaluations of potential biases will need to consider a much wider range of sensitivities to potential uncertainties in emissions and model resolution in the source regions.

Although we have demonstrated that the model can reproduce the distribution of ozone reasonably well, it is clear from both the LIDAR profiles and the ozonesondes that there is a great deal of small-scale structure and layering in the troposphere that is beyond the ability of CTMs to capture at current resolutions. A key question is whether the averaging inherent in these (and other) CTMs is sufficient to capture the mean impacts of precursors on oxidant abundances on the correct temporal and spatial scales. This issue will be addressed in future work.

Acknowledgments. This work was supported by the NASA Tropospheric Chemistry Program as part of the TRACE-P mission. The authors thank the TRACE-P scientists and mission managers for the opportunity to participate in the field deployment. The authors are grateful to the NASA/GSFC TOMS Ozone Processing Team for access to the TOMS ozone column products, to V. Brackett (NASA Langley) for assembling the ozonesonde database, and to the Hong Kong Observatory, the Japan Meteorological Agency, the Central Weather Bureau of Taiwan and Pusan National University for providing ozonesonde data over the TRACE-P period. The ECMWF forecast data were generated under Special Project spnoo3cl at the ECMWF.

Notes

1. Supporting material is available via Web browser or via Anonymous FTP from ftp://ftp.agu.org, directory "apend" (Username = "anonymous", Password = "guest"); subdirectories in the ftp site are arranged by paper number. Information on searching and submitting electronic supplements is found at http://www.agu.org/pubs/esupp_about.html.

References

Andreae, M.O. and P. Merlet, Emissions of trace gases and aerosols from biomass burning, *Global Biogeochemical Cycles, 15,* 955–966, 2001.

Austin, J.F., and R.P. Midgley, The climatology of the jet stream and stratospheric intrusions of ozone over Japan, *Atmos. Environ., 28,* 39–52, 1994.

Berntsen, T., I.S.A. Isaksen, W.C. Wang, and X.Z. Liang, Impacts of increased anthropogenic emissions in Asia on tropospheric ozone and climate, *Tellus, Ser. B, 48,* 13–32, 1996.

Berntsen, T.K. and I.S.A. Isaksen, A global three-dimensional chemical transport model for the troposphere .1. Model description and CO and ozone results, *J. Geophys. Res., 102,* 21239–21280, 1997

Bregman, A., M.C. Krol, H. Teyssedre, W.A. Norton, A. Iwi, M. Chipperfield, G. Pitari, J.K. Sundet, and J. Lelieveld, Chemistry-transport model comparison with ozone observations in the midlatitude lowermost stratosphere, *J. Geophys. Res.*, *106*, 17,479–17,496, 2001.

Browell, E., et al., Large-scale air mass characterization observed over the Western Pacific during TRACE-P, *J. Geophys. Res.*, *this issue*.

Carver, G.D., P.D. Brown and O. Wild, The ASAD atmospheric chemistry integration package and chemical reaction database, *Computer Physics Communications*, *105*, 197–215, 1997.

Douglass, A.R., C.J. Weaver, R.B. Rood, and L. Coy, A three-dimensional simulation of the ozone annual cycle using winds from a data assimilation system, *J. Geophys. Res.*, *101*, 1463–1474, 1996.

Fuelberg, H.E., C.M. Kiley, J.R. Hannan, D.J. Westberg, M.A. Avery, and R.E. Newell, Atmospheric transport during the Transport and Chemical Evolution over the Pacific (TRACE-P) experiment, *J. Geophys. Res.*, *this issue*.

Gauss, M., et al., Radiative forcing in the 21st century due to ozone changes in the troposphere and the lower stratosphere, *J. Geophys. Res.*, accepted Nov 2002.

Hannegan, B.J., Studies of atmospheric trace gases using an improved three-dimensional global chemistry transport model, Ph.D. thesis, University of California, Irvine, 2000.

Hesstvedt, E., Ø. Hov, and I.S.A. Isaksen. Quasi-steady-state approximation in air pollution modelling: comparison of two numerical schemes for oxidant prediction, *Int. J. Chem. Kinet.*, *10*, 971–994, 1978.

Holtslag, A.A.M., E.I.F. Debruijn, and H.L. Pan, A high-resolution air-mass transformation model for short-range weather forecasting *Mon. Weath. Rev.*, *118* 1561–1575, 1990.

Jacob, D.J., J.A. Logan, and P.P. Murti, Effect of rising Asian emissions on surface ozone in the United States, *Geophys. Res. Lett., 26,* 2175–2178, 1999

Jacob, D.J. et al., The Transport and Chemical Evolution over the Pacific (TRACE-P) mission: Design, execution and overview of results, *J. Geophys. Res., this issue*.

Kiley, C., H.E. Fuelberg, D.J. Jacob, P.I. Palmer, K.E. Pickering, D.J. Allen, G.R. Carmichael, T.D. Fairlie, C. Mari, R.B. Pierce, O. Wild, J. Logan, D.G. Streets, and Y. Tang, A comparison of several chemical transport models with aircraft derived plumes of CO from East Asia during the Spring 2001 NASA/TRACE-P Mission, *J. Geophys. Res., this issue*.

McLinden, C.A., S. Olsen, B. Hannegan, O. Wild, M.J. Prather, and J. Sundet, Stratospheric ozone in 3-D models: A simple chemistry and the cross-tropopause flux, *J. Geophys. Res., 105,* 14,653–14,665, 2000.

Olivier, J.G.J., et al., Description of EDGAR Version 2.0, RIVM/TNO report 771060 002, RIVM, Bilthoven, December 1996.

Olivier, J.G.J. and J.J.M. Berdowski, Global emissions sources and sinks, in *The Climate System*, edited by J. Berdowski, R.Guicherit, and B.J. Heij, pp. 33–78, A.A. Balkema Publishers, Lisse, The Netherlands, 2001.

Olsen, S.C., C.A. McLinden, and M.J. Prather, The stratospheric N2O-NOy system: Testing uncertainties in a 3-D framework, *J. Geophys. Res., 106,* 28,771–28,784, 2001.

Oltmans, S.J., B.J. Johnson, J.M. Harris, A.M. Thompson, J.H. Kim, L.Y. Chan, J.P. Chen, et al., Tropospheric ozone over the North Pacific during TRACE-P from ozonesonde observations, *J. Geophys. Res., this issue*.

Prather, M.J., Numerical advection by conservation of second-order moments, *J. Geophys. Res., 91,* 6671–6681, 1986.

Prather, M.J., and D. Ehhalt, Atmospheric Chemistry and Greenhouse Gases, in Climate Change 2001: The Scientific Basis, Cambridge University Press, Cambridge, U.K., 2001.

Prather, M., M. McElroy, S. Wofsy, G. Russell, and D. Rind, Chemistry of the global troposphere: Fluorocarbons as tracers of air motion, *J. Geophys. Res.*, *92*, 6579–6613, 1987.

Streets, D.G., T.C. Bond, G.R. Carmichael, S.D. Fernandes, Q. Fu, D. He, Z. Klimont, S.M. Nelson, N.Y. Tsai, M.Q. Wang, J.-H. Woo, and K.F. Yarber, An inventory of gaseous and primary aerosol emissions in Asia in the year 2000, *J. Geophys. Res.*, *this issue*.

Sundet, J., Model studies with a 3-D global CTM using ECMWF data, Ph.D. Thesis, University of Oslo, Norway, 1997.

van Aardenne, J.A., G.R. Carmichael, H. Levy, D. Streets, and L. Hordijk, Anthropogenic NO_x emissions in Asia in the period 1990–2020, *Atmos. Environ.*, *33*, 633–646, 1999.

Wang, Y.H., D.J. Jacob, and J.A. Logan, Global simulation of tropospheric O3-NOx-hydrocarbon chemistry, 1, Model formulation, *J. Geophys. Res.*, *103*, 10,713–10,725, 1998.

Wild, O., and M.J. Prather, Excitation of the primary tropospheric chemical mode in a global 3-D model, *J. Geophys. Res.*, *105*, 24,647–24,660, 2000.

Wild, O., and H. Akimoto, Intercontinental transport of ozone and its precursors in a 3-D global CTM, *J. Geophys. Res.*, *106*, 27,729–27,744, 2001.

Wild, O., X. Zhu and M.J. Prather, Fast-J: Accurate simulation of in- and below-cloud photolysis in tropospheric chemical models, *J. Atmos. Chem.*, *37*, 245–282, 2000.

Table 1. Ozonesonde Launch Sites Around the North Pacific, February–April 2001

Site	Location	Number
Sapporo, Japan	43.1°N 141.3°E	10
Tateno, Japan	36.1°N 140.1°E	27
Cheju, Korea	33.5°N 126.5°E	9
Kagoshima, Japan	31.6°N 130.6°E	10
Naha, Japan	26.2°N 127.7°E	11
Taiwan	25.0°N 121.4°E	14
Hong Kong	22.3°N 114.2°E	8
Hilo, Hawaii	19.4°N 155.0°W	25
Trinidad Head, CA	40.8°N 124.2°W	23

Figure 1. The latitudinal gradient in ozone column over the western Pacific region (90°–180°E) in March 2001 from TOMS (grey) and the FRSGC/UCI CTM (black). The zonal mean over all longitudes for the same period (dashed) is shown for comparison. Vertical bars indicate the rms variance over the range of longitudes and time.

Figure 2. Total ozone columns for selected days during the campaign compared with concurrent columns from the TOMS instrument. Note that the orbits precess from east to west, covering the region shown in about 10 hours, with the final, westernmost orbital typically at about 4:00 GMT; comparisons are shown at or soon after this to minimize the phase lag.

Figure 3. Comparison of ozone profiles from the FRSGC/UCI CTM (black, dashed) and Oslo CTM2 (grey, dashed) with ozonesonde profiles (solid lines) during the TRACE-P campaign period in 2001. Profiles over the eastern Pacific are available from the FRSGC/UCI CTM only.

Figure 4. Altitude distribution of the 150 ppb isopleth of ozone from all ozonesondes over the North Pacific between February and April 2001, against those from the FRSGC/UCI CTM (left) and Oslo CTM2 (right).

Figure 5. Mean boundary layer ozone below 800 hPa from the FRSGC/UCI CTM against that from all ozonesondes over the North Pacific between February and April 2001 (left) and from the Oslo CTM2 (right).

Figure 6. Ozonesonde profiles of ozone (left) and relative humidity (right) over Taiwan and Hong Kong (solid lines), against those from the FRSGC/UCI CTM (dashed lines). The stratospheric component of modelled ozone is shown in grey.

Figure 7. Comparison of FRSGC/UCI CTM and LIDAR ozone profiles for selected flights across the Pacific from/to Hawaii (Flights 5, 18), from Hong Kong (Flight 7) and from Yokota (Flight 14). Modelled ozone in the stratosphere below 18 km is masked at 500 ppb. The flight track of the DC-8 is shown in white, and black contours indicate approximate cloud optical extinction (10^{-5} cm^{-1}) from the IFS fields.

Figure 8. Decomposition of the ozone profile from the FRSGC/UCI CTM into stratospheric (left panel) and tropospheric (right panel) components. The upper half of each panel shows the flight track profile; the lower half shows slices over the western Pacific at 500 hPa (5 km) and 320 hPa (8 km) four hours into the flight. The flight track of the DC-8 is shown in white, and black contours show mean sea-level pressure from the IFS fields.

Figure 9. Impacts on the ozone profile at Cheju on March 1 of varying the location and time in sampling the FRSGC/UCI CTM fields. The location is varied by one grid box (1.9°) spatially, and the time by 6 hours; successive profiles (black) are shifted by 100 ppb and are shown against the ozonesonde profile (grey). A second ozonesonde, on March 2, is shown for comparison as '+24hr' in the lowest panel, shifted by 550 ppb.

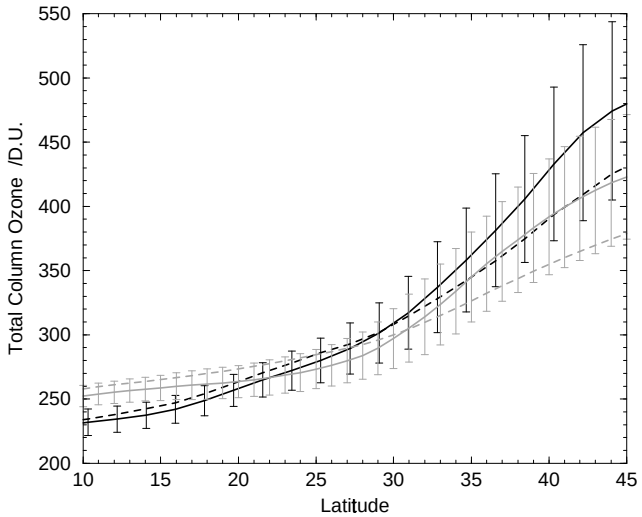

Figure 1. The latitudinal gradient in ozone column over the western Pacific region (90°–180°E) in March 2001 from TOMS (grey) and the FRSGC/UCI CTM (black). The zonal mean over all longitudes for the same period (dashed) is shown for comparison. Vertical bars indicate the rms variance over the range of longitudes and time.

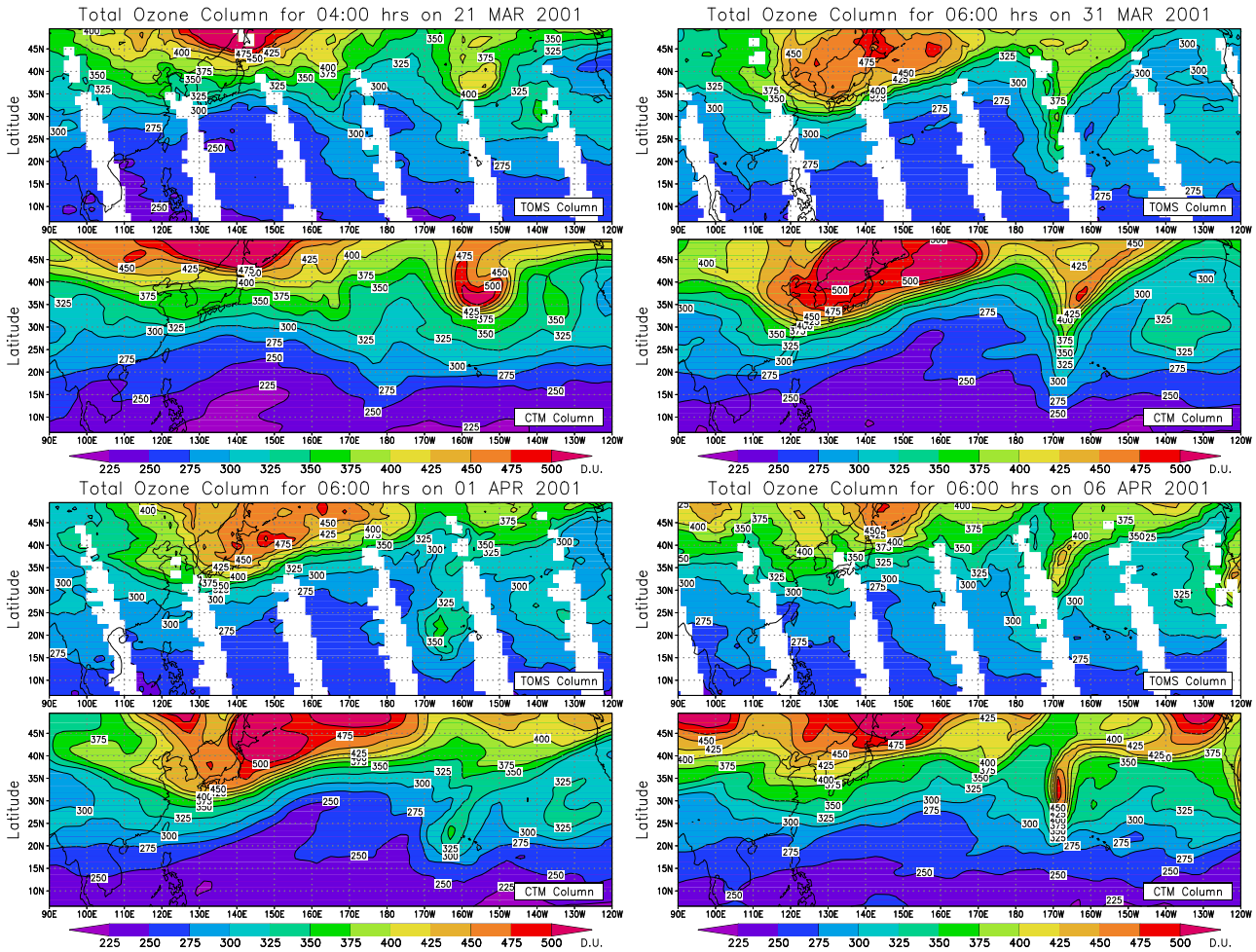

Figure 2. Total ozone columns for selected days during the campaign compared with concurrent columns from the TOMS instrument. Note that the orbits precess from east to west, covering the region shown in about 10 hours, with the final, westernmost orbital typically at about 4:00 GMT; comparisons are shown at or soon after this to minimize the phase lag.

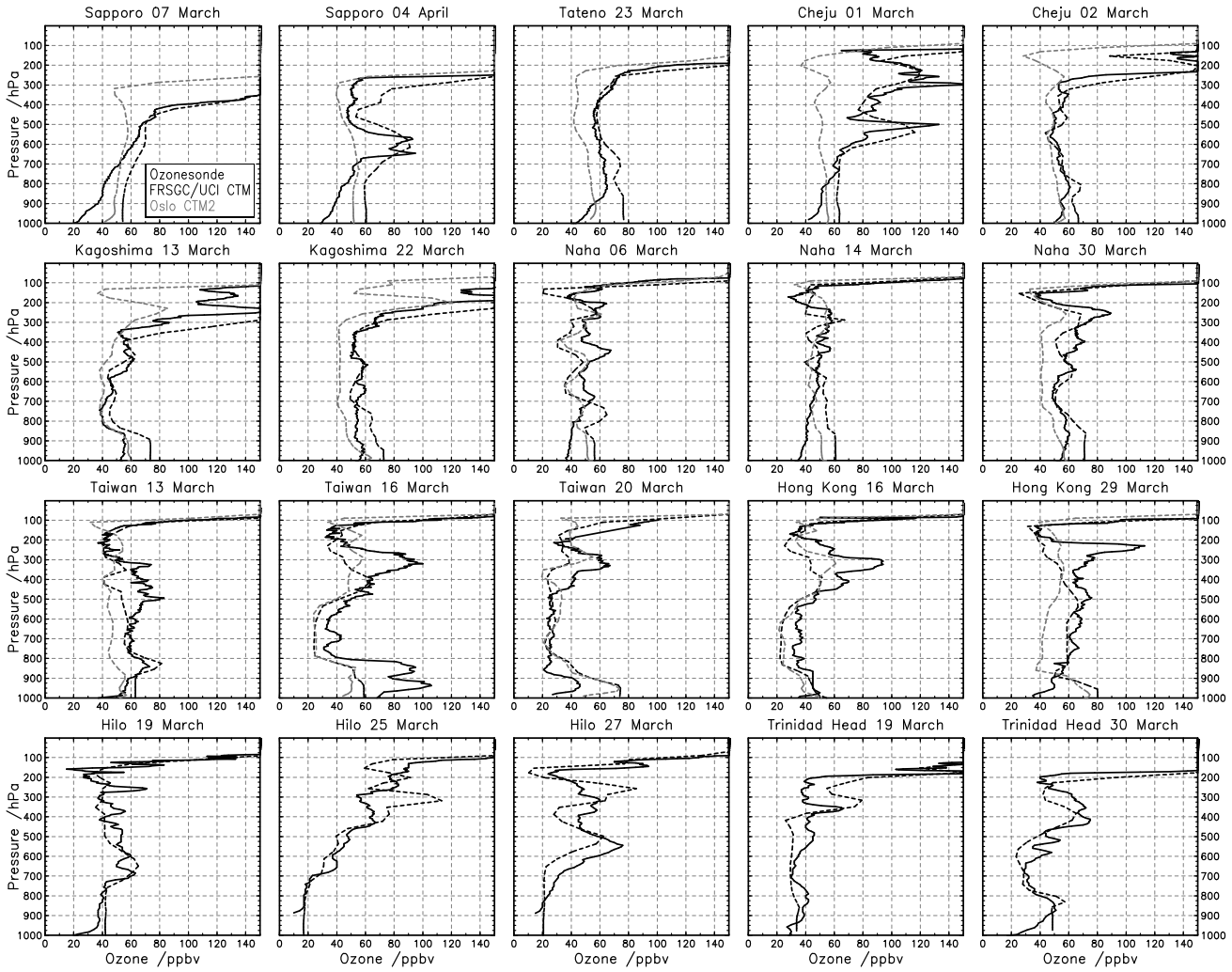

Figure 3. Comparison of ozone profiles from the FRSGC/UCI CTM (black, dashed) and Oslo CTM2 (grey, dashed) with ozonesonde profiles (solid lines) during the TRACE-P campaign period in 2001. Profiles over the eastern Pacific are available from the FRSGC/UCI CTM only.

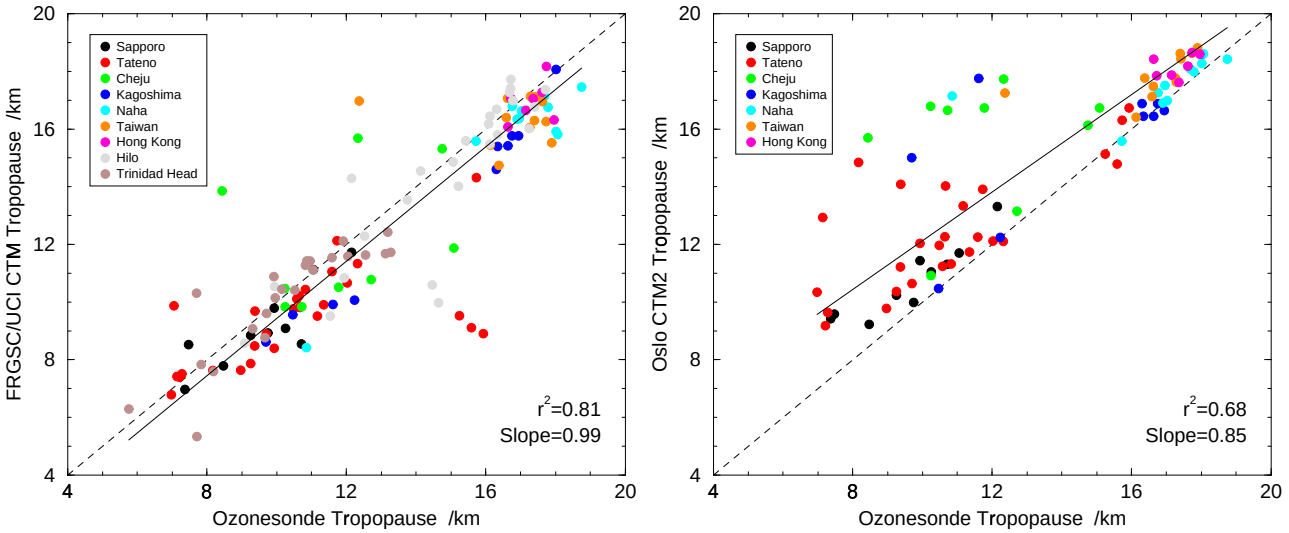

Figure 4. Altitude distribution of the 150 ppb isopleth of ozone from all ozonesondes over the North Pacific between February and April 2001, against those from the FRSGC/UCI CTM (left) and Oslo CTM2 (right).

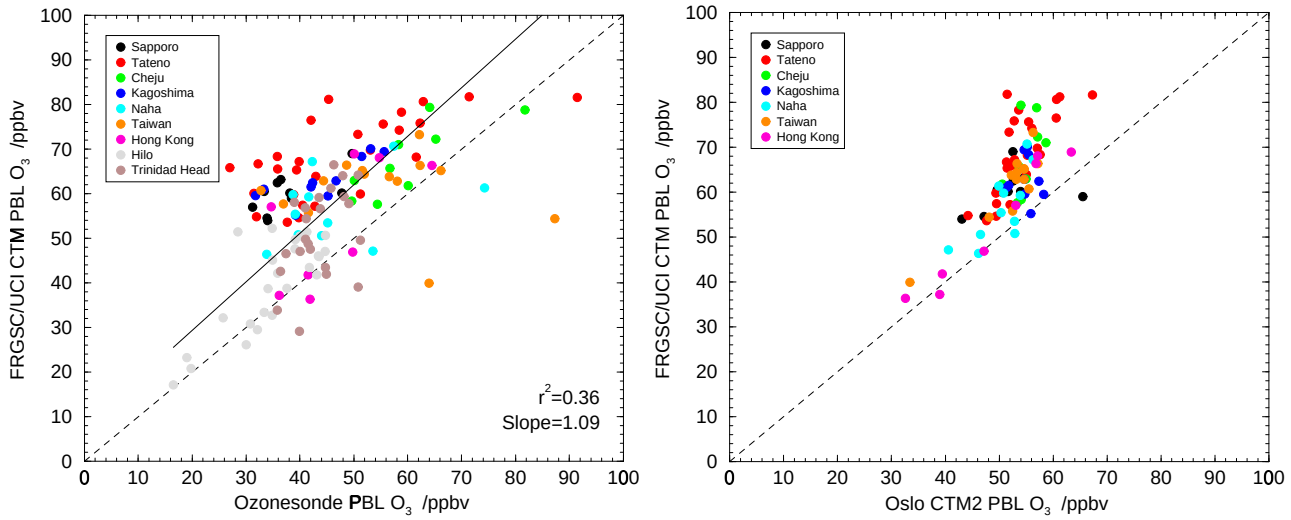

Figure 5. Mean boundary layer ozone below 800 hPa from the FRSGC/UCI CTM against that from all ozonesondes over the North Pacific between February and April 2001 (left) and from the Oslo CTM2 (right).

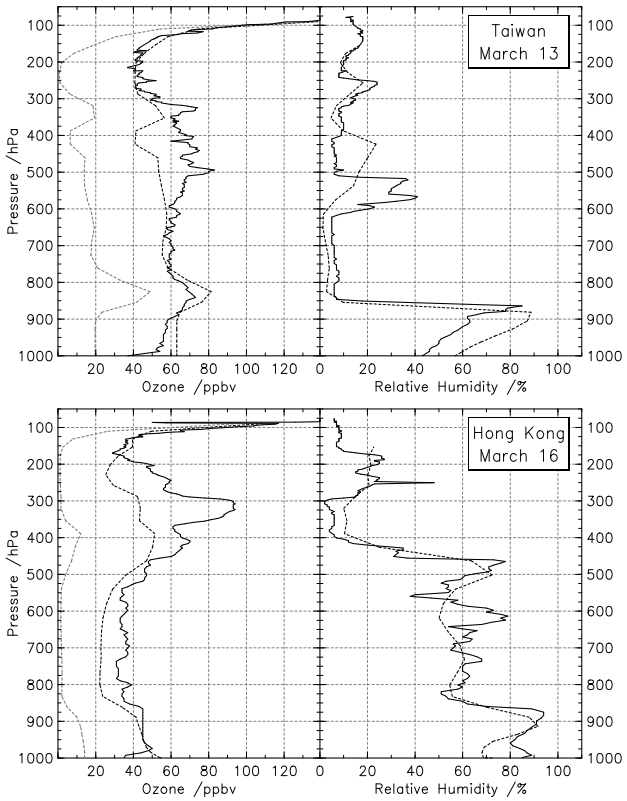

Figure 6. Ozonesonde profiles of ozone (left) and relative humidity (right) over Taiwan and Hong Kong (solid lines), against those from the FRSGC/UCI CTM (dashed lines). The stratospheric component of modelled ozone is shown in grey.

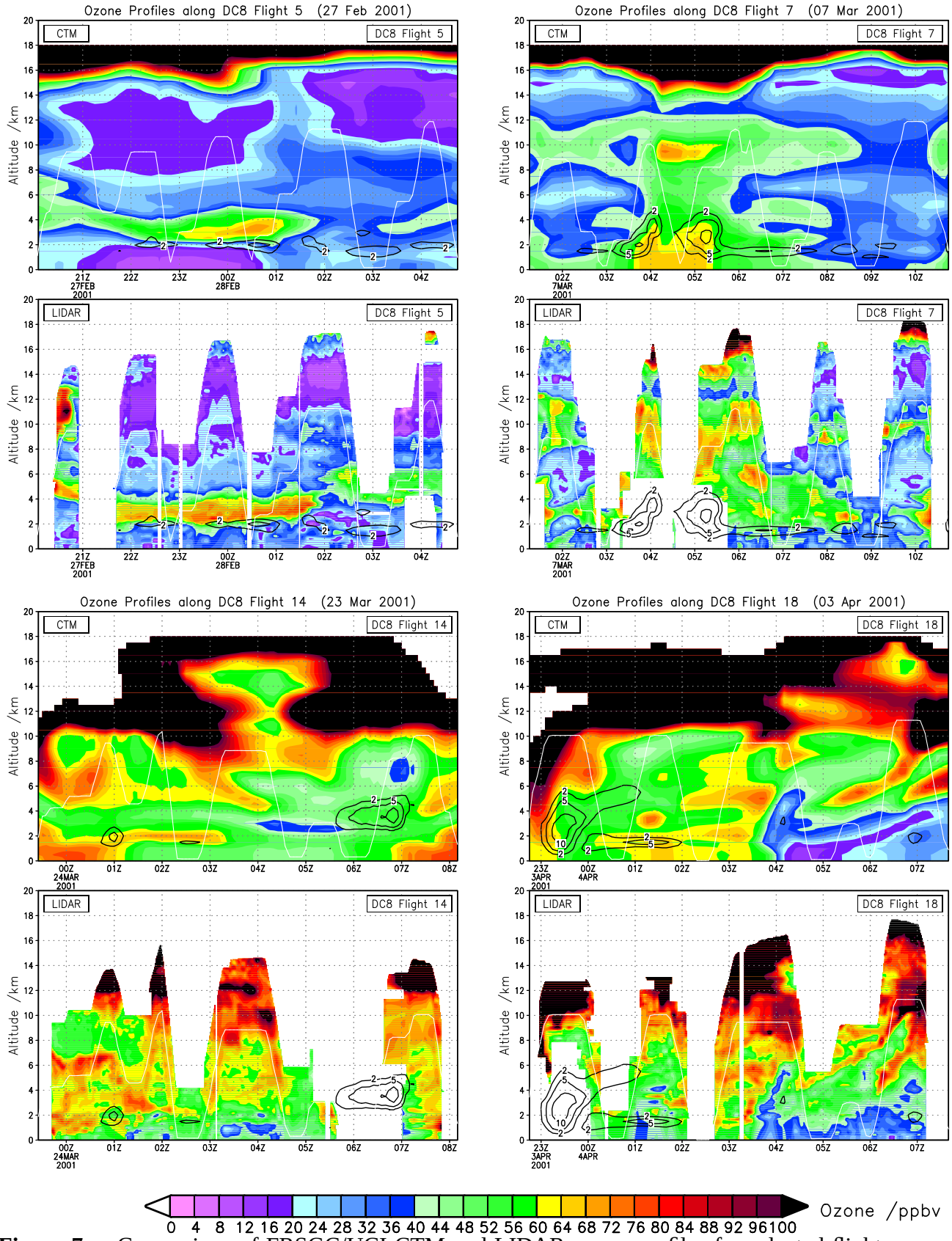

Figure 7. Comparison of FRSGC/UCI CTM and LIDAR ozone profiles for selected flights across the Pacific from/to Hawaii (Flights 5, 18), from Hong Kong (Flight 7) and from Yokota (Flight 14). Modelled ozone in the stratosphere below 18 km is masked at 500 ppb. The flight track of the DC-8 is shown in white, and black contours indicate approximate cloud optical extinction (10^{-5} cm^{-1}) from the

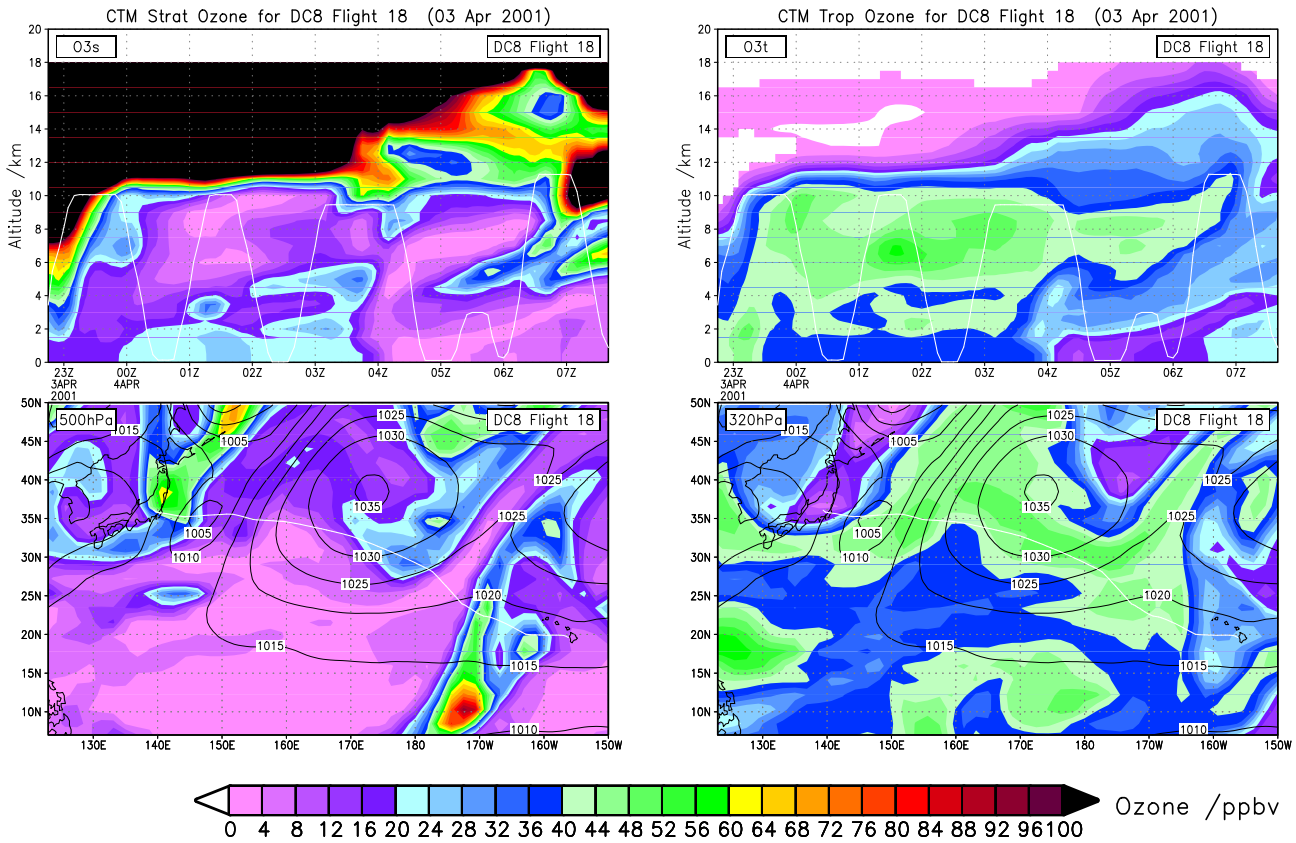

Figure 8. Decomposition of the ozone profile from the FRSGC/UCI CTM into stratospheric (left panel) and tropospheric (right panel) components. The upper half of each panel shows the flight track profile; the lower half shows slices over the western Pacific at 500 hPa (5 km) and 320 hPa (8 km) four hours into the flight. The flight track of the DC-8 is shown in white, and black contours show mean sea-level pressure from the IFS fields.

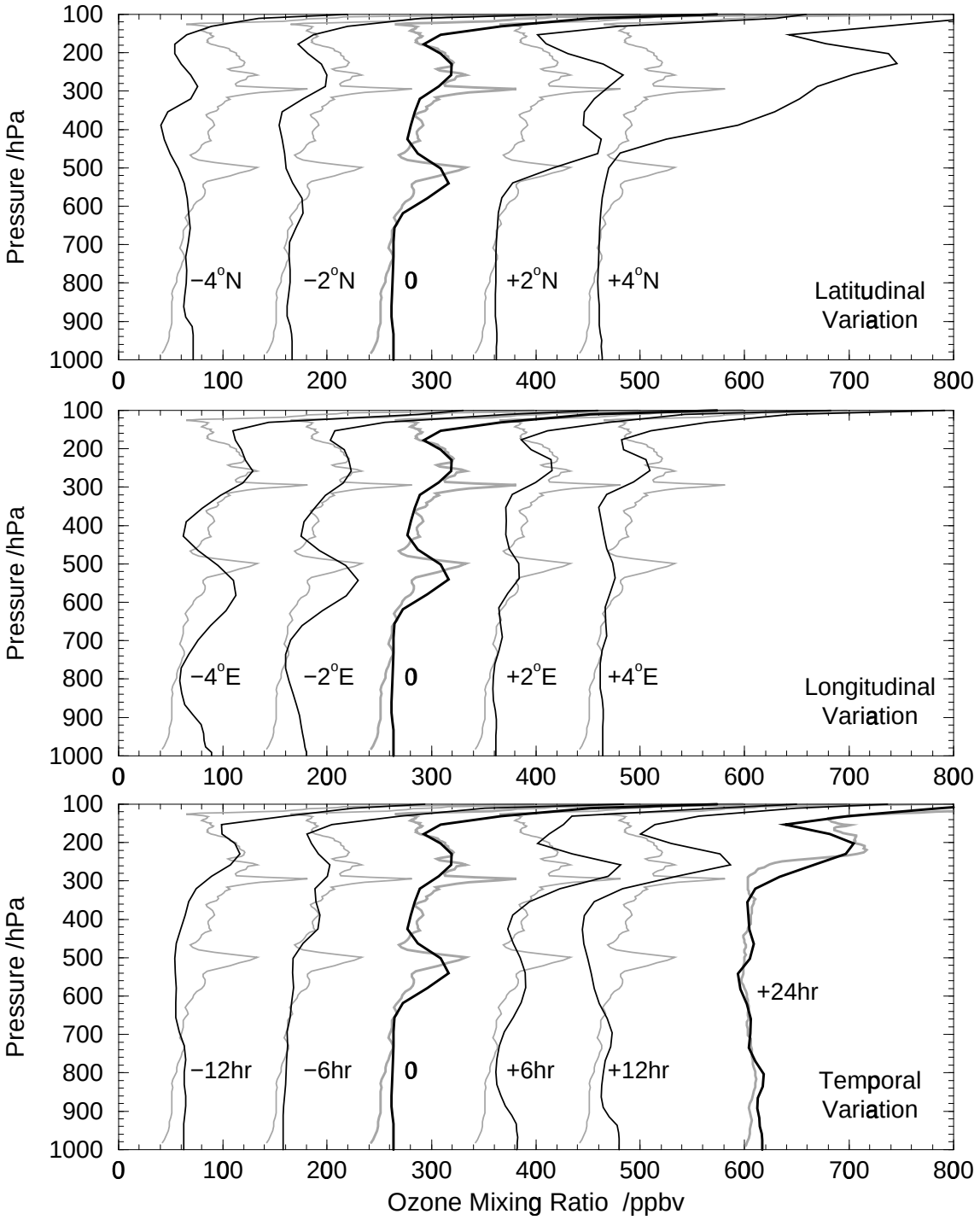

Figure 9. Impacts on the ozone profile at Cheju on March 1 of varying the location and time in sampling the FRSGC/UCI CTM fields. The location is varied by one grid box (1.9°) spatially, and the time by 6 hours; successive profiles (black) are shifted by 100 ppb and are shown against the ozonesonde profile (grey). A second ozonesonde, on March 2, is shown for comparison as '+24hr' in the lowest panel, shifted by 550 ppb.